Toward a unified high-pressure drop model for spray simulations

By J. C. Oefelein and S. K. Aggarwal†

This research focuses on the development of a unified drop vaporization model for use in simulations of high-pressure spray combustion processes. Emphasis is placed on the analysis of supercritical and transcritical processes. These processes occur when a liquid drop that is initially at a subcritical temperature is injected into a high-pressure gaseous environment that exceeds the thermodynamic critical pressure of the interfacial mixture. For this situation the gas-liquid interface undergoes what is commonly referred to as a transcritical heating process. This process is dominated by thermodynamic nonidealities and transport anomalies. Classical models derived using the quasi-steady approximation fail in this limit because of the fundamental assumption that drop vaporization rates are dominated by quasi-steady convective processes. In the transcritical limit, drop vaporization rates are dominated by unsteady diffusion processes. These rate-limiting modes represent two extremes. Here we investigate these extremes by presenting the results from a series of direct numerical simulations. Emphasis is placed on the existence of two rate-limiting parameters and on obtaining a unified approach for modeling the transitional behavior of vaporizing drops over a range of pressures from atmospheric to supercritical.

1. Introduction

Transcritical drop vaporization occurs when the surface of a drop, initially at a subcritical temperature, reaches the critical mixing state (where both phases of the interfacial mixture exist in equilibrium simultaneously) sometime during its lifetime. As a drop evolves in a supercritical ambient, its temperature starts increasing due to heat transfer from the ambient, and vaporization is initiated. Since the drop surface has the highest liquid temperature, it attains the critical mixing state sometime during the drop lifetime. As the the surface approaches the critical mixing state, both surface tension and enthalpy of vaporization go to zero, solubility effects become important, and interfacial boundary conditions change significantly. The subsequent drop regression process is qualitatively different from that in the subcritical state.

A major difficulty in modeling transcritical vaporization stems from the fact that it is governed by processes which are fundamentally different from those which occur at subcritical or "low-pressure" conditions. As a consequence, the classical, quasi-steady, low-pressure models (see for example Godsave (1953), Spalding (1953), Faeth (1977), Law (1982), Faeth (1983), Sirignano (1983), Aggarwal, Tong & Sirignano (1984), Faeth (1987)) can not be used to describe this transcritical behavior. The fundamental difficulty with the classical models in the transcritical limit can be best illustrated by examining the

† University of Illinois at Chicago

quasi-steady equation for vaporization:

$$\tau_{l,LP} = \frac{d_p^2}{12}\,\frac{Pr_s}{\nu_s}\,\frac{1}{\ln(1+B_{T,LP})} \tag{1.1}$$

where the thermal transfer number $B_{T,LP}$ is given by

$$B_{T,LP} = \frac{C_p(T_\infty - T_s)}{\Delta h_{v_p}} \tag{1.2}$$

Here d_p^2 represents the drop diameter, Pr_s the Prandtl number defined at the drop surface, and ν_s the kinematic viscosity at the drop surface. The terms C_p and Δh_{v_p} in Eq. (1.2) represent the constant pressure specific heat and enthalpy of vaporization, respectively. The term T_∞ represents the ambient temperature, and T_s the drop surface temperature. As the drop surface approaches the critical mixing state, C_p approaches infinity and Δh_{v_p} approaches zero, making the transfer number go to infinity. This condition implies that the vaporization rate becomes infinitely fast when in reality there is still a finite-rate effect.

Other fundamental differences between classical low-pressure and high-pressure vaporization phenomena include thermodynamic nonidealities and transport anomalies in the vicinity of gas-liquid interfaces. Interfacial mixture properties exhibit liquid-like densities and gas-like diffusivities. Solubility effects, which are typically negligible at low pressures, become essential considerations at high pressures. Treatment of interfacial thermodynamics becomes significantly more complex and liquid mass transport in the drop interior becomes important. The collective effect of these differences significantly enhances transient effects and drop deformation processes, and the quasi-steady approximation becomes invalid. A quantitative investigation of the quasi-steady assumption for high-pressure conditions has been reported recently by Zhu, Reitz & Aggarwal (2001).

Several recent studies (Shuen, Yang & Hsiao (1992), Jia & Gogos (1993), Givler & Abrahm (1996), Zhu & Aggarwal (2000), Yang (2000)) have focused on transcritical and supercritical vaporization phenomena and have considered many of the high-pressure effects outlined above. Comprehensive reviews of these investigations are provided by Givler & Abrahm (1996) and Yang (2000). Generally, a transient, spherically-symmetric model has been formulated to simulate gas- and liquid-phase processes associated with a drop evaporating in an ambient whose pressure and temperature exceed the critical values of the liquid. High-pressure effects such as gas-phase nonidealities, liquid-phase solubility of gases, and liquid-vapor equilibrium have been represented using appropriate cubic equations of state, or modified Benedict-Webb-Rubin equations of state, along with consistent sets of mixing rules for multicomponent mixtures.

The current investigation focuses on drops that are initially in a subcritical state and are introduced into a gaseous supercritical environment. For this set of conditions, drop surface mixture properties undergo transient heating and mass exchange processes that initially exhibit the classical low-pressure trends given by Eq. (1.1), then, after a period of time, transition to highly transient diffusion dominated processes. This transition occurs when the drop surface attains the critical mixing state. At this point, Eq. (1.1) fails and transcritical vaporization processes dominate at finite-rates.

The objective of this research is to characterize both modes of vaporization and the time-history effect associated with the transition process between these modes. We consider n-hexane–nitrogen systems over the range of pressures, temperatures, and thermodynamic regimes given in Fig. 1. The approach is based on previous work done by Zhu,

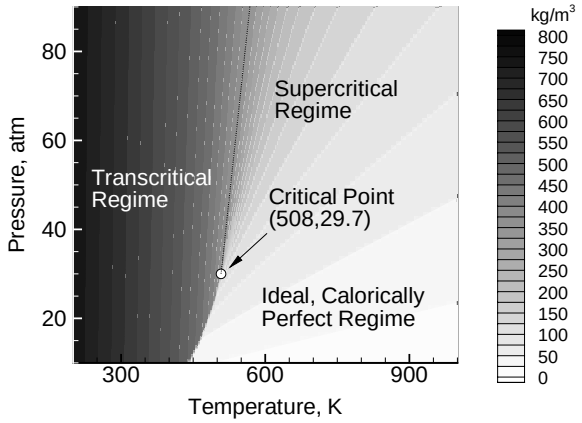

FIGURE 1. Contours of density as a function of pressure and temperature for n-hexane. The critical temperature and pressure is 508 K and 29.7 atm, respectively.

Reitz & Aggarwal (2001), Zhu & Aggarwal (2000), Yang (2000) and Oefelein (1997). We focus on two distinct issues. The first is on the development of a general correlation which is analogous to Eq. (1.1) and can be used to characterize vaporization rates above over a range of ambient conditions from atmospheric to supercritical. The second is on the development of a model which characterizes the associated transitional time-history effects. The goal is to develop a model that is sufficiently simple so that it can be feasibly applied in large-scale spray simulations in a manner analogous to the widely used low-pressure models.

2. Theoretical-numerical framework

The analysis was conducted by performing a series of direct numerical simulations (DNS) using two established theoretical-numerical frameworks, one developed by Oefelein (1997), the other by Zhu & Aggarwal (2000). Both frameworks solve the fully-coupled conservation equations of mass, momentum, total energy, and species for both the gas and liquid phases and take full account of gas-liquid interface dynamics.

The framework developed by Oefelein (1997) uses an extended corresponding states principle similar to that developed by Rowlinson & Watson (1969) to model thermophysical mixture properties over the relevant range of pressures and temperatures. A 32-term Benedict-Webb-Rubin (BWR) equation of state similar to that developed by Jacobsen & Stewart (1973) is used to predict PVT behavior for real gas, liquid, or gas-liquid mixtures. Enthalpy, Gibbs energy, and the constant pressure specific heat are obtained as a function of temperature and pressure using thermodynamic departure functions. Viscosity and thermal conductivity are obtained in a similar manner using the methodologies developed by Ely and Hanley Ely & Hanley (1981a), Ely & Hanley (1981b), Ely & Hanley (1981c). The effective mass diffusion coefficients are calculated using two models. Gas phase quantities, as dictated by phase equilibrium theory, are evaluated using the mixing rules given by Bird, Stewart & Lightfoot (1960) coupled with Chapman-Enskog theory, the Lennard-Jones intermolecular potential function Wilke & Lee (1955), and a high-pressure correction proposed by Takahashi (1974). Liquid phase quantities are evaluated

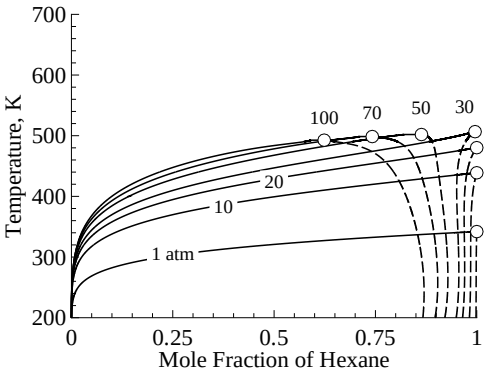

FIGURE 2. Vapor-liquid phase equilibrium composition for an n-hexane–nitrogen system at different pressures. Symbols: – – – – , liquid; ——— , vapor; ∘ , critical mixing state.

using the mixing rules proposed by Perkins and Geankoplis Reid, Prausnitz & Poling (1987) and Hayduk & Minhas (1982).

The framework developed by Zhu & Aggarwal (2000) uses a similar property evaluation scheme but with a Peng-Robinson (PR) equation of state to represent nonideal behavior. This framework uses an arbitrary Lagrangian-Eulerian (ALE) numerical method which allows a dynamically adaptive mesh to be used to analyze interfacial time-history effects as a function of various initial conditions. For this situation transport across the discontinuity is balanced by the continuity of mass and energy fluxes and the condition of phase equilibrium. The accuracy of this scheme and that described above has been demonstrated in the works cited. Figure 1, for example, was obtained using the 32-term BWR equation of state with the corresponding states principle. This methodology has been shown to model the PVT behavior of liquid, vapor, and gaseous hydrocarbon mixtures to factors well within 2% of measured values. It is particularly accurate in the difficult region near the critical point. The PR equation of state exhibits similar accuracy but is slightly less accurate in its ability to map liquid-gas saturation properties.

3. Results and discussion

The modeled system is an isolated liquid-hexane drop surrounded by nitrogen gas in a spherically-symmetric domain. Calculations were performed by imposing two fundamentally different initial conditions at the drop surface. One set of results were obtained using the framework developed by Oefelein (1997) with the drop surface conditions initialized to the critical mixing state. A second set of results were obtained using the framework developed by Zhu & Aggarwal (2000) with the drop surface conditions initialized using jump conditions balanced by continuity of mass and energy fluxes and the condition of phase equilibrium. These initial conditions represent the limiting extremes. The former yields vaporization rates which are dominated by transient transcritical diffusion processes. The latter yields vaporization rates which are first dominated by quasi-steady subcritical processes, then, after a period of time, become dominated by transient transcritical diffusion processes.

Modeling drop vaporization processes hinges on an accurate representation of the gas-liquid interface. At subcritical conditions, the interface is characterized by jump conditions due to the presence of surface tension. When the critical mixing state is reached,

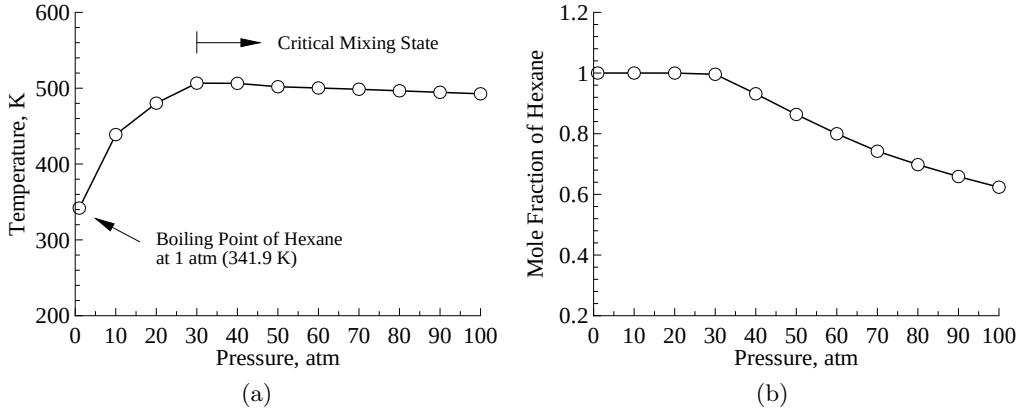

FIGURE 3. Equilibrium mixture temperature (a) and composition (b) as a function of pressure showing the boiling line and critical mixing line.

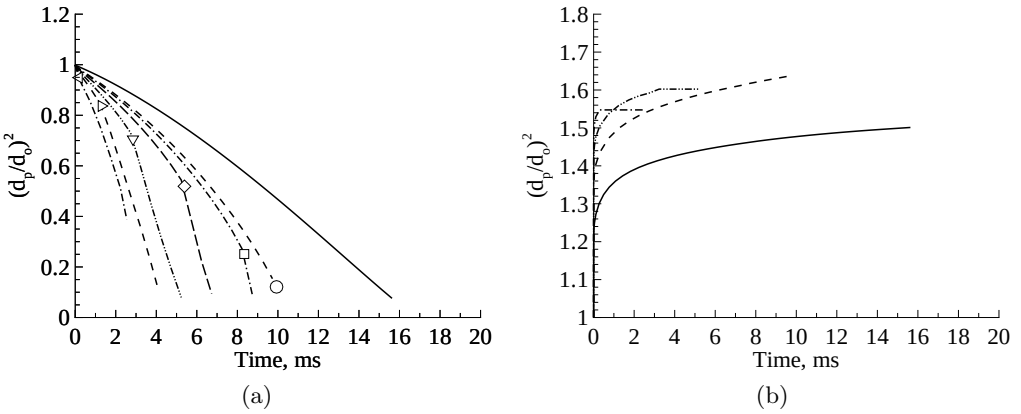

FIGURE 4. Temporal variation of the dimensionless drop surface (a) and surface temperature (b) for an n-hexane–nitrogen system. The initial temperature is 300 K, ambient temperature is 1500 K, and initial drop diameter is 100 μm. Attainment of the critical mixing state is represented with symbols. (a): ——— , 30; ○ , 90, ◘ ; 100, ◇ , 120; ▽, 150; ▷, 180; ◁, 220. (b): ——— , 30; – – – – , 90; —··— , 150; —·— , 220.

however, the drop surface becomes indistinguishable from the gas phase and subsequent drop regression is characterized by the motion of the critical surface. This surface is characterized by assuming that the interfacial mixture is in a state of thermodynamic equilibrium. Figure 2 shows the calculated equilibrium composition for an n-hexane–nitrogen system over the relevant range of pressures. The dashed lines represent the liquid phase, the solid lines represent the vapor phase, and the symbols represent the critical mixing state, which is the only point on the curve where both vapor and liquid can exist in equilibrium simultaneously. The locus of points represent the critical mixing state. These points are plotted in Fig. 3. The curve to the left of the critical pressure gives n-hexane boiling temperatures as a function of pressure. The curve to the right gives the critical mixing state as a function of pressure. In this limit, all other thermophysical surface properties can be calculated as a function of these primitives.

Figure 4 shows the dual modes of vaporization that can occur when drop surface conditions are initialized using jump conditions. Here the temporal variation of the di-

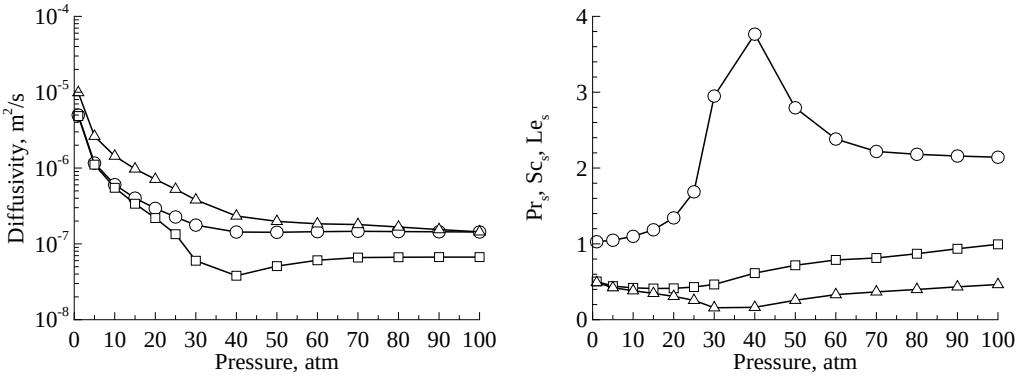

FIGURE 5. Mean variation in kinematic viscosity ν_s thermal diffusivity α_s and mass diffusivity $\mathcal{D}_{ij}$ (a) and the corresponding Prandtl, Schmidt, and Lewis numbers (b) as a function of pressure for an n-hexane–nitrogen system with initial liquid and ambient temperatures of 300 and 1500 K, respectively. Symbols: (a) ○ , ν_s; □ , α_s; △, D_{ij}. (b) ○ , Pr_s; □ , Sc_s; △, Le_s.

mensionless surface area and surface temperature is given for a range of pressures which includes both the quasi-steady subcritical and the transient transcritical vaporization regimes. These histories have been validated with measurements reported by Nomura, Ujiie, Rath, Sato & Kono (1996). The attainment of the critical mixing state is indicated by respective symbols. Prior to reaching this state, drop vaporization rates are dominated by quasi-steady convective processes that are characterized quite accurately by Eq. (1.1). Upon reaching the critical mixing state, however, a distinct change in the vaporization rate occurs and Eq. (1.1) is no longer valid. The time associated with this transition can be significant.

3.1. *Correlation for transcritical vaporization*

Subcritical vaporization rates are well characterized by Eq. (1.1). This classic equation implies that drops vaporize according to a d_p^2 law and that the rate of vaporization for a fixed diameter is inversely proportional to the product of the thermal diffusivity at the surface and the term $\ln(1 + B_{T,LP})$, where $B_{T,LP}$ is the thermal transfer number given by Eq. (1.2). $B_{T,LP}$ is directly proportional to the product of the constant pressure specific heat and the temperature difference between the drop surface and ambient gas, and inversely proportional to the enthalpy of vaporization. Figures 5 and 6 show how the diffusion coefficients, enthalpy of vaporization, and surface tension vary as a function of pressure for a representative n-hexane–nitrogen system.

Difficulties arise with Eq. (1.1) in the limit as the drop surface approaches the critical mixing state. In this limit drop surface properties (as characterized by the pressure, temperature, and composition given in Fig. 3) become invariant with time and the drop surface regression rate is determined by the rate at which the critical surface moves inward. The diffusion coefficients remain well behaved, but the enthalpy of vaporization (which dominates relative to the rise in C_p) becomes zero. This drives Eq. (1.2) toward infinity, and, as a consequence, Eq. (1.1) incorrectly predicts the occurrence of an infinitely fast vaporization rate. In reality finite-rate effects are still prevalent.

Yang (2000) has identified two rate limiting parameters which can be used to quantify finite-rate vaporization processes in the transcritical limit. The first is a correction due to the spatial variation in thermal diffusivity which occurs between the ambient gas and

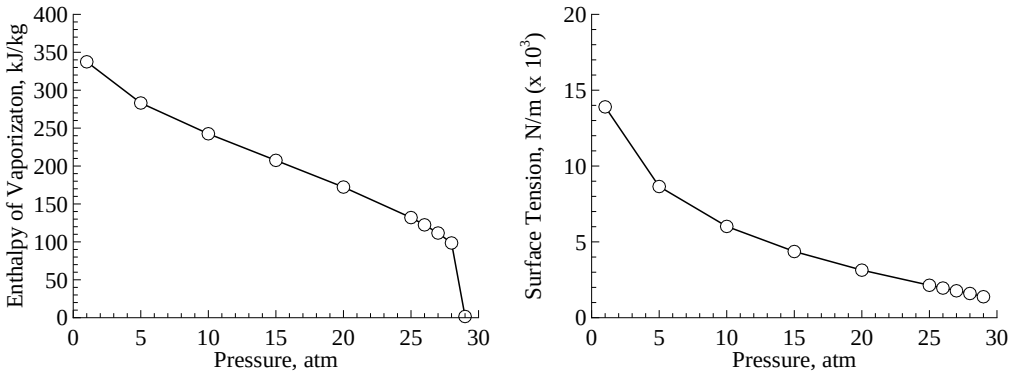

FIGURE 6. Mean variation in enthalpy of vaporization Δh_{v_p} (a) and surface tension σ_s (b) as a function of pressure for an n-hexane–nitrogen system with initial liquid and ambient temperatures of 300 and 1500 K, respectively.

drop. The second is a transfer number based on the critical mixing temperature:

$$B_{T,HP} = \frac{T_\infty - T_{cm}}{T_{cm} - T_p} \tag{3.1}$$

where T_∞ represents the ambient temperature, T_{cm} the critical mixing temperature, and T_p the temperature of the drop. The utility of these parameters has been validated for liquid-oxygen–hydrogen systems. The correction associated with the thermal diffusivity characterizes the limiting behavior of transient diffusion processes at the critical surface. Equation (3.1) characterizes the limiting behavior of energy exchange processes across the drop surface.

To obtain a general correlation, an expression analogous to Eq. (1.1) was sought that exhibited the correct limiting behavior over the interval $0 \leq B_T < \infty$. This expression was obtained by solving the transient heat conduction equation for a solid sphere initially at a uniform temperature T_o in a quiescent ambient gas initially at a uniform temperature T_∞. After solving for the reduced temperature $(T_\infty - T)/(T_\infty - T_o)$ as a function of time and space, the resultant expression is integrated over the dimensionless time interval $0 \leq \tau^\star \leq \tau_l^\star$ to obtain an expression for the dimensionless drop life time:

$$\tau_l^\star = \frac{\tau_l}{d_o^2/\alpha_o} \tag{3.2}$$

This solution is obtained in a manner consistent with the behavior of the critical interface by assuming that the surface temperature is constant. For this set of conditions, the reduced drop lifetime is only a function of the reduced interface temperature. This expression is given as:

$$(T_\infty - T_{cm})/(T_\infty - T_o) = B_{T,HP}/(1 + B_{T,HP}) \tag{3.3}$$

and, as shown above in Eq. (3.3), is directly related to the high-pressure transfer number defined by Eq. (3.1). The final solution is given by:

$$\frac{B_{T,HP}}{1 + B_{T,HP}} = \operatorname{erf}\left(\frac{1}{\sqrt{4\tau_l^\star}}\right) - \frac{1}{\sqrt{\pi\tau_l^\star}} \exp\left(\frac{1}{\sqrt{4\tau_l^\star}}\right) \tag{3.4}$$

TABLE 1. Curve fit coefficients corresponding to Eqs. (3.5) (and (3.6)) for the interval $0 \leq B_T < \infty$.

	Set 1	Set 2	Set 3	Set 4
a_0	1.00×10^{0}	8.44×10^{-1}	5.37×10^{-1}	2.77×10^{-1}
a_1	1.94×10^{0}	3.36×10^{-1}	3.07×10^{-2}	1.76×10^{-3}
a_2	1.12×10^{1}	1.78×10^{-1}	1.82×10^{-3}	1.08×10^{-5}
a_3	5.22×10^{1}	6.88×10^{-2}	7.37×10^{-5}	4.43×10^{-8}
a_4	1.63×10^{2}	1.81×10^{-2}	1.99×10^{-6}	1.20×10^{-10}
a_5	3.35×10^{2}	3.21×10^{-3}	3.58×10^{-8}	2.18×10^{-13}
a_6	4.44×10^{2}	3.76×10^{-4}	4.23×10^{-10}	2.58×10^{-16}
a_7	3.64×10^{2}	2.78×10^{-5}	3.14×10^{-12}	1.93×10^{-19}
a_8	1.68×10^{2}	1.17×10^{-6}	1.33×10^{-14}	8.18×10^{-23}
a_9	3.35×10^{1}	2.15×10^{-8}	2.46×10^{-17}	1.51×10^{-26}

Set 1:	$0 \leq 1/\ln(1+B_T) < 1$	$1.718 \times 10^{0} \leq B_T < \infty$
Set 2:	$1 \leq 1/\ln(1+B_T) < 10$	$1.052 \times 10^{-2} \leq B_T < 1.718 \times 10^{0}$
Set 3:	$10 \leq 1/\ln(1+B_T) < 100$	$1.005 \times 10^{-2} \leq B_T < 1.052 \times 10^{-1}$
Set 4:	$100 \leq 1/\ln(1+B_T) < 1000$	$0 \leq B_T < 1.005 \times 10^{-2}$

This equation establishes an analytic relation between the transfer number and the dimensionless drop lifetime.

The roots of Eq. (3.4) must be obtained numerically. After performing this operation and analyzing various trends, a functional dependence of the form:

$$\ln(1+B_T)\ \tau_l^\star = \sum_{n=0}^{9} (-1)^n \frac{a_n}{[\ln(1+B_T)]^n} \tag{3.5}$$

was obtained. The coefficients corresponding to this equation are given in Table 1. This equation approaches 0 in the limit as $B_T \to 0$, and 1 in the limit as $B_T \to \infty$. It is also interesting to note that for $a_0 = 1$ and $a_n = 0$ (n = 1–9), this equation reduces to the same form as Eq. (1.1). These well bounded characteristics suggest a correlation of the form:

$$\tau_{l,HP} = \frac{d_p^2}{12}\ \frac{Pr_s}{\nu_s}\ \frac{1}{\ln(1+B_{T,HP})}\ f\left(\frac{\alpha_s}{\alpha_p}\right)\ \sum_{n=0}^{9} (-1)^n \frac{a_n}{[\ln(1+B_T)]^n} \tag{3.6}$$

where here the time constant in Eq. (3.2) was replaced with the ratio d_p^2/α_s (with α_s represented above using the definition of the Prandtl number) and a correction factor of the form $f(\alpha_s/\alpha_p)$ was applied to account for the spatial variation in the thermal diffusivity. This variation is not accounted for in the analytic approximation.

To validate Eq. (3.6) a set of 43 simulations were performed. The matrix of cases considers pressures of 40, 50, 60, 70, 80, 90, and 100 atm with initial ambient temperatures of 600, 900, 1200, 1500, 1800 and 2100 K. In all cases the initial drop temperature was 300 K. Dimensional analysis shows that the initial drop diameter is the only length scale and that the drop lifetime is proportional to the diameter-squared. Thus only drops with an initial diameter of 100 μm are considered in the present analysis. The resultant drop lifetimes are plotted in Fig. 7a. To analyze the effectiveness of Eq. (3.6), the drop lifetimes plotted in Fig. 7a were compared to respective predictions using a fitted value

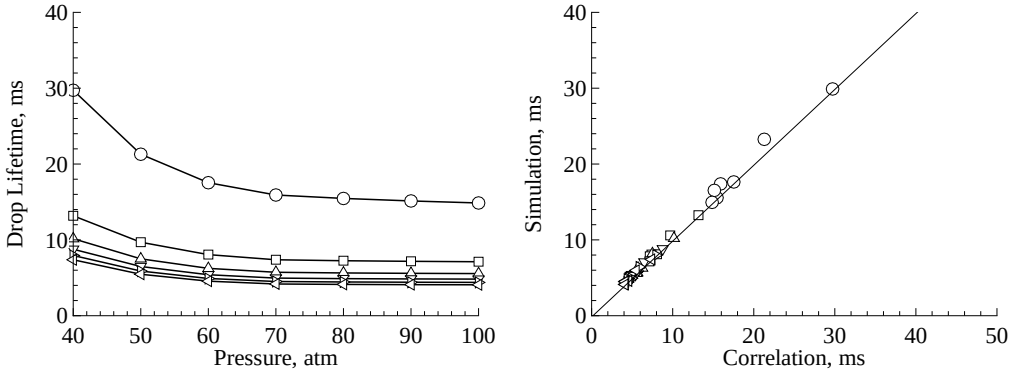

(a) (b)

FIGURE 7. Transcritical drop lifetime as a function of pressure and temperature (a) and comparison of the vaporization rate given by DNS versus the correlation given by Eq. (3.6) (b). The initial drop temperature is 300 K. The initial drop diameter is 100 μm. $T_\infty = \circ$, 600K; $\square$, 900K; $\triangle$, 1200K; $\triangledown$, 1500K; $\triangleright$, 1800K; $\triangleleft$, 2100K.

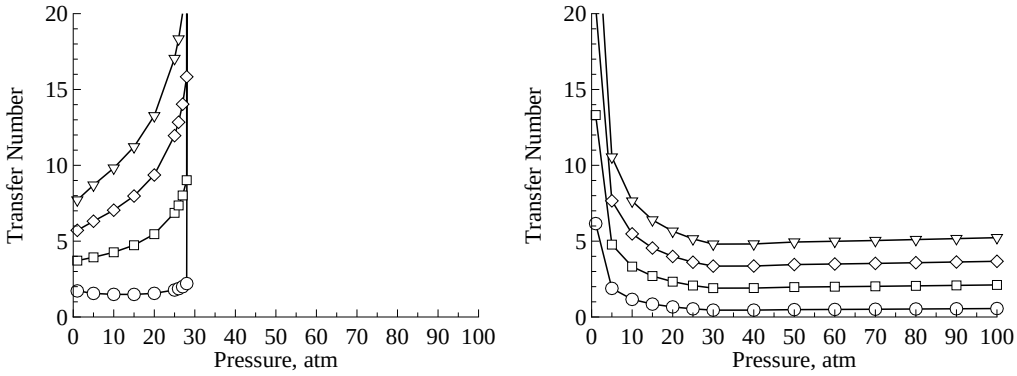

(a) (b)

FIGURE 8. Mean variation of transfer number based on the classical low-pressure definition given by Eq. (1.2) (a) and the critical mixing temperature as given by Eq. (3.1) (b) as a function of pressure. $T_\infty = \circ$, 600K; $\square$, 900K; $\diamond$, 1200K; $\triangledown$, 1500K.

of $f(\alpha_s/\alpha_p) = 1.2$. This comparison is plotted in Fig. 7b, which shows respective drop vaporization rates given by the DNS compared with the corresponding rate given by Eq. (3.6). A least-squares fit of these data indicate that the agreement is within a margin of 5 percent.

3.2. *Transitional behavior of the transfer number*

Figure 8 shows the mean variation of transfer number based on the classical low-pressure definition, as given by Eq. (1.2), and the critical mixing temperature, as given by Eq. (3.1). The results exhibit several interesting trends. Fig. 8a shows that the low-pressure transfer number is strongly dependent on both pressure and ambient temperature. At 1 atm, this quantity is well behaved and varies from approximately 1.75 to 7.75 when the ambient gas temperature is varied from 600 to 1500 K. In the limit as pressure approaches the critical pressure of n-hexane, the low-pressure transfer number goes to infinity since the enthalpy of vaporization goes to zero. In contrast, the high-pressure transfer number

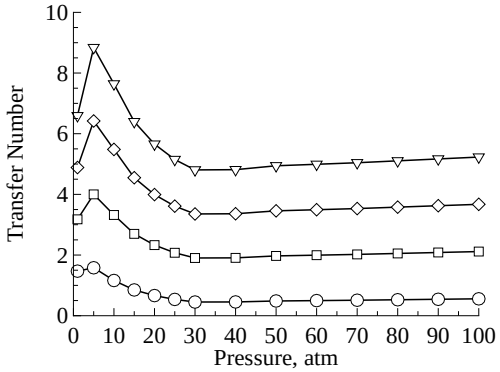

FIGURE 9. Composite transfer number obtained by evaluating Eq. (3.7) using the data given in Fig. 8. $T_\infty = \circ$, 600K; $\square$, 900K; $\diamond$, 1200K; ∇, 1500K.

goes to infinity in the limit as pressure approaches zero, and it is well behaved as the pressure approaches infinity. At pressures above critical, there is a strong sensitivity to the ambient gas temperature but not to pressure. Here a variation from approximately 1 to 6 occurs when the ambient gas temperature is varied from 600 to 1500 K.

A last observation regarding Fig. 8 is that respective curves associated with the low and high transfer numbers intersect at the same pressure (7 atm for the conditions considered here). This implies that the transitional process from the low- to high-pressure transfer numbers is independent of both temperature and pressure and is only a function of the critical mixing pressure. This suggests that the transition process can be handled by using a transfer number defined as the minimum of the low-pressure and high-pressure values:

$$B_T = \min(B_{T,LP}, B_{T,HP}) \tag{3.7}$$

This equation incorporates transitional effects with the correct limiting behavior for pressure approaching 0 and ∞. It also peaks at the correct value of 7 atm; however, this may represent an overprediction. This detail will be addressed in future work. Figure 9 shows the composite transfer number corresponding the the results given in Fig. 8.

3.3. *Transitional time-history effects*

Equation (3.6) characterizes the transcritical mode of vaporization but not the time-history effects described above. The trends shown in Fig. 4 illustrated this effect quite clearly. For the cases shown, the drop never attains the critical mixing state at pressures below 90 atm. At pressures above 90 atm, the drop undergoes transcritical vaporization sometime during its lifetime. As pressure increases, this transition or the attainment of the critical mixing state occurs progressively earlier in its lifetime. At 220 atm, the drop attains the critical mixing state almost instantaneously.

The total drop lifetime, defined here as τ_v, consists of 1) the time to reach the critical mixing state τ_c, which decreases with pressure, and 2) the time associated with transcritical regression, which also decreases with pressure. To characterize the effects of ambient and drop properties on the attainment of the critical mixing state, we examine the ratio of the time to attain the critical mixing state relative to the total drop lifetime. Figure 10 shows the variation of this ratio as a function of pressure for different ambient temperatures and initial drop diameters. As τ_c/τ_v goes to unity, the drop surface regression is characterized completely by a subcritical vaporization process. As this ratio goes to zero,

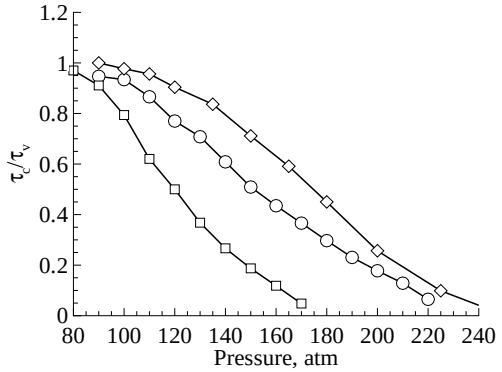

FIGURE 10. Ratio of time for an n-hexane drop to reach the critical mixing state versus total lifetime. Symbols: ○ , $100\mu m$, 1500K; □ , $100\mu m$, 2000K; ◇ , $200\mu m$, 1500K.

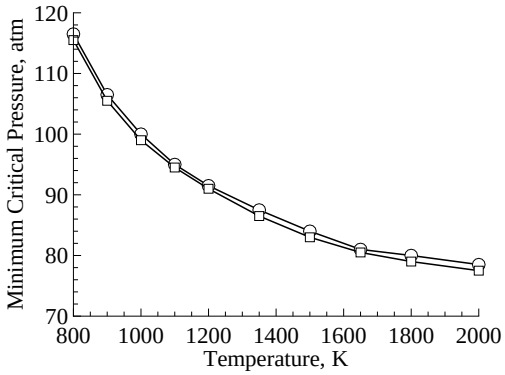

FIGURE 11. Minimum pressure required for an n-hexane drop to attain the critical mixing state. Symbols: ○ , $d_p = 100\mu m$; ◘ , $d_p = 100\mu m$.

the surface regression process is characterized completely by transcritical vaporization processes. This ratio decreases with pressure, which implies that τ_c decreases faster than τ_v. The time ratio parameter also decreases as the ambient temperature is increased and as the initial drop diameter is decreased. Both of these effects can be attributed to an inherent decrease in the drop heat-up time.

In Fig. 11, we plot the minimum pressure required for the attainment of critical mixing state as a function of ambient temperature. In order to obtain a minimum pressure value at a fixed ambient temperature, simulations were performed for increasingly higher pressures until a critical mixing state is observed at the drop surface. Thus, the curve in Fig. 11 represents a boundary between the subcritical and transcritical vaporization. Any point above the curve indicates that the critical mixing state will be reached sometime during the drop lifetime. The further a point is from the curve in the supercritical region, the smaller the ratio τ_c/τ_v, which implies the drop attains the critical mixing state earlier in its lifetime. On the other hand, any point below the curve corresponds to a condition of subcritical vaporization where τ_c/τ_v is one and the drop never attains the critical mixing state. This relation is useful in identifying the subcritical and supercritical vaporization regimes in a more quantitative manner. Another important observation from Fig. 11 is

that the minimum pressure required for the attainment of the critical mixing state is independent of the initial drop diameter.

4. Conclusions

This work represents a first step toward the development of a unified high-pressure drop model for spray simulations. The key trends have been quantified and a general correlation has been developed and validated for n-hexane–nitrogen systems. Key trends associated with the transfer number were also established over a relevant range of pressures and were shown to be bounded in the transcritical limit. Issues associated with surface heating and ambient conditions were also identified and analyzed.

To complete the model, this work must be extended to establish the quantitative variation in transfer number for mixing states in the transitional region that occurs at pressures between atmospheric and critical. The time-history associated with surface heating must be incorporated with companion correlations to account for convective effects in the ambient gas and subcritical and transcritical drop deformation processes.

Acknowledgments

Partial support for this work was provided by the Center for Integrated Turbulence Simulations under the U.S. Department of Energy Accelerated Strategic Computing Initiative and by the Center for Turbulence Research.

REFERENCES

Aggarwal, S. K., Tong, A., & Sirignano, W. A. 1984 A comparison of vaporization models in spray calculations. *AIAA J.* **22**, 1448-1457.

Bird, R. B., Stewart, W. E. & Lightfoot, E. N. 1960 *Transport phenomena*. Wiley New York, New York.

Ely, J. F. & Hanley, H. J. M. 1981a An enskog correction for size and mass difference effects in mixture viscosity predictions. *J. of Research of the National Bureau of Standards.* **86**(6), 597-604.

Ely, J. F. & Hanley, H. J. M. 1981b Predictions of transport properties. 1. Viscosity of fluids and mixtures. *Industrial and Engineering Chemistry Fundamentals.* **20**(4), 323-332.

Ely, J. F. & Hanley, H. J. M. 1981c Predictions of transport properties. 2. Thermal conductivity of pure fluids and mixtures. *Industrial and Engineering Chemistry Fundamentals.* **22**(4), 90-97.

Faeth, G. M. 1977 Current Status of Droplet and Liquid Combustion. *Prog. Energy & Combust. Sci.* **3**, 191-224.

Faeth, G. M. 1983 Evaporation and Combustion of Sprays. *Prog. Energy & Combust. Sci.* **9**, 1-76.

Faeth, G. M. 1987 Mixing, Transport, and Combustion in Sprays. *Prog. Energy & Combust. Sci.* **13**, 293-345.

Givler, S. D. & Abraham, J. 1996 Supercritical droplet vaporization and combustion studies. *Prog. Energy & Combust. Sci.* **22**, 1-28.

Godsave, G. A. E. 1953 Studies of the combustion of drops in a fuel spray - the burning

of single drops of fuel. *Fourth Symposium (International) on Combustion*, Williams and Wilkins, Baltimore, MD, 818-830.

Hayduk, W. & Minhas, B. S. 1982 Correlations for prediction of molecular diffusivities in liquid. *Canadian J. of Chem. Eng.* **60**, 295-299.

Jia, H. & Gogos, G. 1993 High-pressure droplet vaporization; Effects of liquid-phase gas solubility. *Int. J. Heat & Mass Transfer* **36** 4419-4431.

Jacobsen, R. T. & Stewart, R. B. 1973 Thermodynamic properties of nitrogen including liquid and vapor phases from 63K to 2000K with pressure to 10,000 bar. *J. of Phys. and Chem. Ref. Data.* **2**(4), 757-922.

Law, C. K. 1982 Recent advances in droplet vaporization and combustion. *Prog. Energy & Comb. Sci.* **8**, l71-201.

Matlosz, R. L., Leipziger, S., & Torda, T. P. 1972 Investigation of liquid drop evaporation in a high temperature and high pressure environment. *Int. J. Heat & Mass Transfer.* **15**, 831-852.

Nomura, H., Ujiie, Y., Rath, H. J., Sato, J. & Kono, M. 1996 Experimental study of high-pressure droplet evaporation using microgravity conditions. *Twenty-Sixth Symposium (International) on Combustion*, The Combustion Institute, Pittsburgh, 1267-1273.

Oefelein, J. C. 1997 *Simulation and analysis of turbulent multiphase combustion processes at high pressures.* Ph.D. Thesis, The Pennsylvania State University, University Park, PA.

Reid, R. C., Prausnitz, J. M. & Poling, B. E. 1987 *The properties of gases and liquids.* McGraw-Hill Book Company.

Rowlinson, J. S. & Watson, I. D. 1969 The prediction of the thermodynamic properties of fluids and fluid mixtures - I. The principle of corresponding states and its extensions. *Chem. & Eng. Sci.* **24**(8), 1565-1574.

Spalding, D. B. 1953 The combustion of liquid fuels. *Fourth Symposium (International) on Combustion*, Williams and Wilkins, Baltimore, 847-864.

Shuen, J. S., Yang, V., & Hsiao, C. C. 1992 Combustion of liquid-fuel droplets in supercritical conditions. *Combust. & Flame.* **89**, 299-319.

Sirignano, W. A. 1983 Fuel droplet vaporization and spray combustion. *Prog. Energy & Comb. Sci.* **9**, 291-322.

Takahashi, S. 1974 Preparation of a generalized chart for the diffusion coefficients of gases at high pressures. *Japanese J. of Chem. Eng.* **7**(6), 417-420.

Wilke, C. R. & Lee, C. Y. 1955 Estimation of diffusion coefficients for gases and vapors. *Industrial Engineering Chemistry.* **47**, 1253-1257.

Yang, V. 2000 Modeling of supercritical vaporization, mixing, and combustion processes in liquid-fueled propulsion systems. *Twenty-Eighth Symposium (International) on Combustion*, The Combustion Institute, Pittsburgh, in print.

Zhu, G. S. & Aggarwal, S. K. 2000 Transient supercritical droplet evaporation with emphasis on the effects of equation of state. *Int. J. Heat & Mass Transfer.* **43**, 1157-1171.

Zhu, G. S., Reitz, R. D. & Aggarwal, S. K. 2001 Gas-phase unsteadiness and its influence on droplet vaporization in sub- and super-critical environments. To appear in *Int. J. of Heat & Mass Transfer.*